RSC Advances

PAPER

View Article Online
View Journal | View Issue

Check for updates

Cite this: *RSC Adv.*, 2026, **16**, 13320

Environmentally friendly fluorescence platform for detection of tetracycline in pharmaceutical formulations and human serums based on highly fluorescent 1,4-di-2-(5-phenyloxazolyl)-benzene

Muhammad S. Mustafa * and Wrya O. Karim

Tetracycline (TC) is an efficient antibiotic used for curing different bacterial infections in both humans and animals. Accurate and precise detection of TC is a requisite for quality control of pharmaceutical productions and patient safety using a reliable method. This study presents a highly sensitive and selective strategy based on utilizing 1,4-di-2-(5-phenyloxazolyl)-benzene (POB) as a molecular fluorescence sensor for detecting TC. POB displays an optimal excitation and a high-intensity emission at 355 nm and 418 nm, respectively. The TC–POB interaction leads to a remarkable quenching of the fluorescence, allowing fluorometric detection of TC. A linear calibration curve in a range of 0.5–40 μM along with a limit of detection (LOD) of 0.143 μM was established. The analytical applicability of the developed method was estimated for measuring TC within pharmaceutical formulations and human serum samples, revealing high accuracy and precision. Ultimately, the greenness of the proposed method was inspected *via* the Analytical Greenness Metrics for Sample Preparation (AGREEprep) and the Analytical Greenness Index (BAGI), emphasizing the eco-friendly feature with respect to sample preparation steps, applicability, and practicability.

Received 2nd February 2026
Accepted 4th March 2026

DOI: 10.1039/d6ra00893c

rsc.li/rsc-advances

Open Access Article. Published on 09 March 2026. Downloaded on 4/15/2026 7:33:55 PM.
This article is licensed under a Creative Commons Attribution-NonCommercial 3.0 Unported Licence.

1. Introduction

Antibiotics are an essential category of pharmacological agents used to treat infectious diseases in humans and animals that either inhibit bacterial growth (bacteriostatic) or kill bacteria (bactericidal).[1,2] Among these agents, tetracycline (TC) is regarded as a broad-spectrum antibiotic widely used in both human healthcare and livestock production in order to prevent and treat infections caused by pathogenic microorganisms. TC functions effectively by binding it to the 30S ribosomal subunit and blocking the aminoacyl-tRNA attachment, thereby inhibiting bacterial protein synthesis.[3–6] Excessive or inappropriate use of TC can be attributed to serious risks, including hepatotoxicity, nephrotoxicity, delayed tooth development, and the emergence of antimicrobial resistance.[7,8] As documented by Schulz *et al.*, the toxic concentration level of TC in human blood was found to be 67.57 mM, and Liu *et al.* recorded a maximum detected level at 0.75 μM.[9,10] Therefore, according to the above-mentioned arguments, it is highly necessary to establish a robust analytical technique. It is not only an easy and fast approach but also provides an accurate, precise, and reliable methodology for the determination of TC in both pharmaceutical formulations and serum samples.

Tremendous analytical approaches and hyphenated ones are currently available to detect TC in a variety of samples, such as UV-vis spectrophotometry,[11–13] HPLC,[14–20] HPLC-MS/MS,[21–24] electrochemical methods,[25–27] capillary electrophoresis,[28,29] surface-enhanced Raman spectroscopy (SERS),[30] and liquid chromatography-tandem mass spectrometry (LC-MS/MS).[31] Based on its reliability, high specificity and accuracy, and capability to resolve complex mixtures, HPLC is often recognized as the method of choice. On the other hand, HPLC and related methodologies are not free of drawbacks, including the frequent need for labor-intensive sample preparation, high instrumentation costs, time-consuming analysis, and the requirement for a high level of expertise from the experimenter. Most of these limitations have been addressed in fluorescence-based techniques, which offer several distinct merits in terms of selectivity, sensitivity, easy operation, cost-effectiveness, admirable stability, response time, high sampling frequency, direct visual interpretation, and easy signal detection.[32,33] In this regard, there is an increased demand for the development of sophisticated fluorescence-based sensing platforms for TC analysis, which is of considerable interest.

Throughout the literature, numerous fluorophores have been described for the design of fluorescence sensors to quantify TC in diverse sample matrices, such as carbon dots

Department of Chemistry, College of Science, University of Sulaimani, Qliasan St., Kurdistan Region, Sulaymaniyah, 46002, Iraq. E-mail: muhammad.mustafa@univsul.edu.iq

© 2026 The Author(s). Published by the Royal Society of Chemistry

Open Access Article. Published on 09 March 2026. Downloaded on 4/15/2026 7:33:55 PM. This article is licensed under a Creative Commons Attribution-NonCommercial 3.0 Unported Licence.

(CDs), functionalized CDs,[34–38] and metal–organic frameworks (MOFs).[39–41] However, CDs have several drawbacks, such as relatively low quantum yields, unstable fluorescence behaviors, complex surface functionalization regimes, and concerns about reproducibility owing to variability in synthesis.[42–44] Likewise, MOFs have several limitations, such as quenching due to the guest molecules undergoing either oxidative and reduced interaction with the framework, low stability in certain pH conditions or solvents, lack of sufficient chemical selectivity, and high response time due to the hindrance to the diffusion or migration of the analyte by the porous structure.[45,46] Among the fluorescence-based approaches used for such contexts, molecular fluorescence sensors are still considered one of the effective methods. Sensors of this type are composed of small molecules or supramolecular complexes and work as effective analytical tools for quantifying target analytes in various matrices. After these sensors precisely interact with their desired analyte, the change in fluorescence emission will be observed. The change in fluorescence intensity of the sensor is correlated with the quantity of analyte, offering a highly selective and sensitive method for analyte detection.[47–50]

The goal of the present article is to establish and develop a sensitive, convenient, and effective fluorescence-based sensor for TC quantification. For this purpose, a molecular fluorescence sensor based on 1,4-di-2-(5-phenyloxazoyl)-benzene (POB) has been developed as an efficient fluorophore that has a rigid conjugated structure and high quantum yield due to its strong and intense fluorescence, which makes fluorescence change easy to measure. Moreover, POB has exceptional resistance to photobleaching, allowing for prolonged fluorescence stability. TC has multifunctional groups, including hydroxyl, carbonyl, and amide groups, that facilitate interaction with the sensor. Therefore, the fluorescence intensity of the sensor is quenched by the incremental addition of TC under optimized experimental conditions. This provides a selective, sensitive, and straightforward approach for quantifying TC in pharmaceutical products and serum samples. In addition, the proposed fluorometric method demonstrates excellent environmental compatibility, as energy consumption, solvent usage, and waste production were carefully considered and verified by extensive greenness metric analyses.

2. Materials and methods

2.1. Materials

High-purity and analytical-grade chemical reagents were used during all experiments to achieve maximum accuracy and reproducibility. Tetracycline (TC), obtained at Aladdin Ltd, Shanghai, China; 1,4-di-2-(5-phenyloxazolyl)-benzene (POB), toluene (PhMe), cyclohexane (C_6H_{12}), dichloromethane (CH_2Cl_2), chloroform ($CHCl_3$), ethyl acetate (EtOAc), acetonitrile (ACN), ethanol (EtOH), methanol (MeOH), and dimethyl sulfoxide (DMSO) were purchased from Sigma-Aldrich and used as received without further purification. Metal salts $Al(NO_3)_3 \cdot 9H_2O$, $Cr(NO_3)_3 \cdot 9H_2O$, $Mg(NO_3)_3 \cdot 6H_2O$, $Ca(NO_3)_3 \cdot 6H_2O$, $Cd(NO_3)_3 \cdot 4H_2O$, $Ni(NO_3)_3 \cdot 6H_2O$, $MnCl_2 \cdot 4H_2O$, $Cu(NO_3)_2 \cdot 3H_2O$, $Zn(NO_3)_2 \cdot 6H_2O$, $NaNO_3$, KNO_3, $Fe(NO_3)_3 \cdot 9H_2O$, and biomolecules were purchased from local suppliers (Merck, Sigma-Aldrich).

2.2. Instrumentation

Fluorescence lifetime measurements were carried out using an Edinburgh Instruments FLS1000 fluorescence spectrometer (Edinburgh Instruments Ltd, UK) equipped with a time-correlated single-photon counting (TCSPC) module. The analysis of optical properties was performed using a Cary 60 spectrophotometer (Agilent Technologies, USA) to obtain UV–Vis spectra. For acquiring fluorescence excitation and emission spectra, the Cary Eclipse spectrofluorimeter (Agilent Technologies, USA) was used.

2.3. Preparation of standard solutions

The series of solutions were obtained from stock solutions of POB (1000 μM) and TC (1000 μM), which were prepared upon dissolving 36.24 mg of POB and 44.40 mg of TC in 100 mL of ethanol, respectively.

2.4. Fluorescence detection of TC

A 5 mL blank solution was prepared from 0.16 μM POB by diluting 0.8 mL of the 1 μM POB solution. Afterwards, 0.8 mL of the 1 μM POB solution was mixed with varying concentrations of TC, followed by dilution to 5 mL to prepare a series of standard solutions with different TC concentrations. The fluorescence intensity (F_0) of the blank solution (0.16 μM POB) and the fluorescence intensity of the POB (F) after addition of the different TC concentrations were recorded at excitation and emission wavelengths of 355 nm and 418 nm, respectively. A calibration curve was constructed by plotting the ratio of the fluorescence intensity of POB (F_0) to the fluorescence intensity of POB in the presence of TC(F)) against the corresponding concentrations TC. Finally, linear regression equation was computed from the calibration curve.

2.5. Application to pharmaceutical formulation

A local drugstore provided ten capsules of TC as a drug product that were crushed and homogenized into uniform powder. A precise weight of capsule powder was treated by adding ethanol and then sonicated for 10 min to ensure dissolution of the maximum quantity of active constituent. The insoluble excipients were filtered using a 0.45 μM membrane filter. Subsequent dilutions of the clear filtrate were made into ethanol, producing three sample solutions that spanned the concentration range of the TC calibration curve. A known volume of the prepared TC sample solution individually was mixed with the 0.1 mL of the 1 μM POB, followed by dilution to 5 mL. Under the optimum experimental conditions, the fluorescence intensity of POB (F_0) and the fluorescence intensity of POB in the presence of TC (F) were measured. The fluorescence response ratio (F_0/F) for each TC sample solution was computed. The concentration of TC in the pharmaceutical product was quantified from the linear regression equation of the standard calibration curve, and the results were compared with the label claim.

Open Access Article. Published on 09 March 2026. Downloaded on 4/15/2026 7:33:55 PM. This article is licensed under a Creative Commons Attribution-NonCommercial 3.0 Unported Licence.

2.6. Application to spiked human serum

The protein fraction of the biological serum samples was removed quantitatively. Briefly, a mixture of 1 mL of blood serum and 3 mL of acetonitrile was centrifuged for 10 min to precipitate the proteins.[55] The resulting supernatant was collected and subjected to analysis. An aliquot of 50 μL of the supernatant was transferred into a series of volumetric flasks. Subsequently, spiked samples were prepared by adding varying concentrations of a TC standard solution within the established calibration range. The remaining volume was completed with ethanol to reach the final volume. The fluorescence intensity of each spiked sample was recorded and analyzed according to the proposed method. The fluorescence ratio (F_0/F) for each spiked sample solution was manipulated. The concentration of TC in the serum samples were determined from the linear regression equation of the standard calibration curve. Ultimately, the recovery percentages were calculated by comparing the experimentally measured TC concentrations with the known added amounts.

2.7. Quantum yield (QY)

In this study, a common standard fluorescent dye (fluorescein) has a QY of 0.95 in basic media and was utilized as a reference for calculation of QY of the POB.[51] Initially, the emission spectra of the POB and the standard were recorded in the range of 360–600 nm at an optimized excitation wavelength of 355 nm and 495–600 nm at an excitation wavelength of 490 nm, respectively. The absorbance of both the standard and POB was measured at their corresponding excitation wavelengths. Subsequently, the QY of POB was determined using the following equation:

$$\phi_x = \phi_{st} \frac{F_x}{F_{st}} \frac{A_{st}}{A_x} \left(\frac{\eta_x}{\eta_{st}}\right)^2$$

where ϕ_x and ϕ_{st} represent the quantum yields of the sample and standard, respectively. A_x and A_{st} are absorbance values, and F_x and F_{st} are the integrated fluorescence emission spectra, η_x and η_{st} refers to the solvents' refractive indices. Solvents used were distilled water and ethanol with respective indices of 1.33 and 1.36 for the preparation of standard and sample solutions, respectively. The credibility of the results was checked by analyzing samples, and reference solutions of different concentrations were prepared, keeping the optical absorption values between 0 and 0.1. Fluorescence spectra of the two sets of solutions were then recorded, and the quantum yield was determined by the comparison of fluorescence and absorbance.

3. Results and discussion

3.1. Optical properties of POB

Fluorescent sensors have been recognized as an effective tool in analytical chemistry and show high performance for quantifying different desired analytes. Thus, the study of fluorescent materials is fundamental in the field of optical sensors; specifically, these materials absorb ultraviolet light energy and then emit light at different wavelengths. POB is a natural fluorescent polycyclic aromatic compound, exhibiting notable features including high quantum yield, strong and stable emission, broad Stokes shift, and excellent photostability. The chemical structure consists of sp^2-hybridized carbon, nitrogen, and oxygen atoms, demonstrating an elongated π-conjugated system that governs its absorption and emission behaviors. UV-Vis and fluorescence spectroscopy were used for characterizing optical properties of POB and their suitability as a robust fluorescent probe for analytical applications.

As depicted in Fig. 1a, the UV–Vis absorption spectrum of POB shows a broad absorption band in the range from 200 to 400 nm, with a distinct peak at 355 nm and two shoulders at 344 nm and 379 nm. The peak at 355 nm associated with a π–π* electronic transition in the extended conjugated aromatic system, indicating the presence of multiple energy levels for electronic excitation; thereby highlighting a highly delocalized

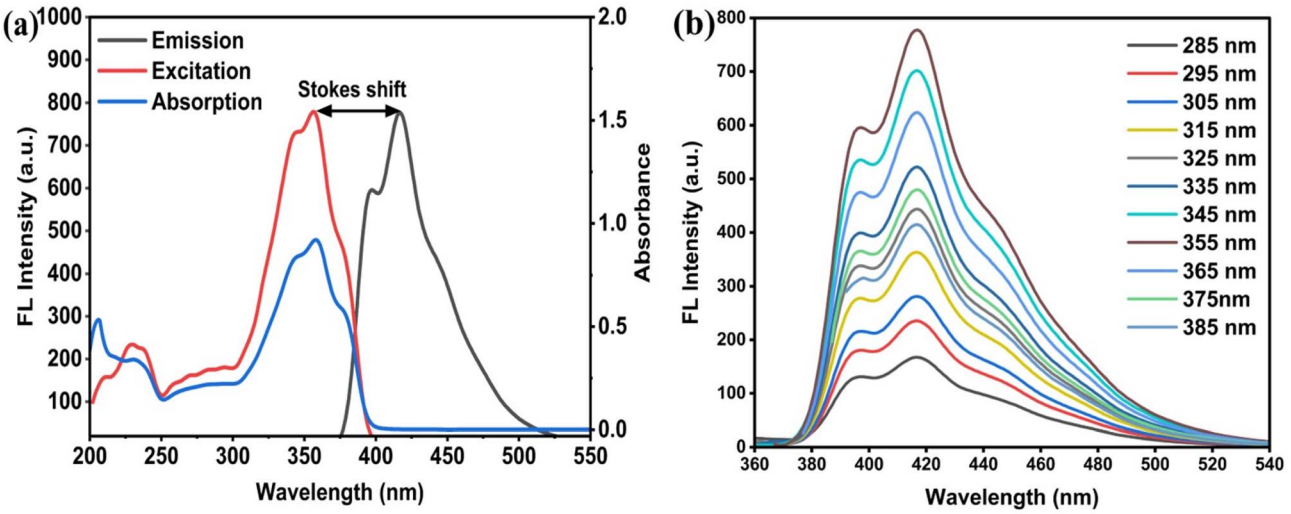

Fig. 1 (a) UV-Vis absorption and fluorescence spectra of 0.16 μM POB; (b) emission spectra of 0.16 μM POB under various excitation wavelengths using ethanol as a solvent.

© 2026 The Author(s). Published by the Royal Society of Chemistry

Open Access Article. Published on 09 March 2026. Downloaded on 4/15/2026 7:33:55 PM.
This article is licensed under a Creative Commons Attribution-NonCommercial 3.0 Unported Licence.

π-electronic system within the aromatic structure. Accordingly, the optical features of POB are predominantly directed by π–π* transitions, with n–π transitions being minimal owing to the insignificant contribution of heteroatoms with lone electron pairs. Furthermore, the absorption and excitation, respectively, as can be seen from the figure, with the excitation spectrum measured by observing the emission at 418 nm, reveal a well-defined peak at 355 nm. Upon excitation at 355 nm, the POB emitted a strong green fluorescence at 418 nm. The Stokes shift of about 63 nm is obviously seen between the wavelengths of excitation (355 nm) and emission (418 nm) maxima, which corresponds to about 4246 cm^{-1}, indicating an efficient relaxation of the excited-state molecules before photon emission.

The fluorescence intensity of the POB was measured under different excitation wavelengths as illustrated in Fig. 1b. The minimal variations in the maximum emission wavelengths suggest the excitation-independent behavior and a single emissive state. More than all these characters, the fluorescence QY of POB reaches 84% at 355 nm, asserting its remarkable efficiency in converting absorbed light to emitted light. The strong absorption, high quantum yield, large Stokes shift, and spectral stability highlight POB's exceptional and desired optical properties. Ultimately, POB is eligible as a fluorescent probe or sensing material in analytical chemistry applications.

3.2. Selectivity of POB for TC

One of the essential optical properties is the selectivity of POB that is demanded for precise and accurate detection of target analytes without interference from other components. Overall, an enhanced, reliable, selective, and sensitive sensor exists. In this work, the selectivity of the POB sensor was assessed in the presence of 0.01 M of common interfering species, including cations, various biomolecules, and several antibiotics. To explore the possible cationic interferences, the fluorescence intensity response of 0.16 μM POB (blank) before and after being subjected to several cations was recorded as portrayed in Fig. 2a. The outcomes reveal the negligibility of the probe responses to these ions, assuring eligibility of various numbers of ionic species.

The tolerance of the sensor toward interferences of biological molecules and various antibiotics was explored (Fig. 2b). Numerous interferents that exist in the pharmaceutical products, including sugars (fructose (Fru), sucrose (Suc), and lactose (Lac)), metabolic compounds (glucose (Glu), uric acid (Ura), urea (Ure), ascorbic acid (Asa)), amino acids (arginine (Arg), tyrosine (Tyr), glycine (Gly), and aspartic acid (Asp)), and antibacterial agents, for example, azithromycin (Azm), ciprofloxacin (Cip), clarithromycin (Clm), vancomycin (Vam), gentamycin (Gem), and tetracycline (TC), were examined. The results show that these compounds experience minimal fluctuations in the fluorescence outcome of 0.16 μM POB (blank). However, TC induces substantial quenching that is taken into consideration during the analysis. This is superior selectivity of POB toward TC over other relevant biochemical species. The analysis of POB reveals suitability for the detection of TC in pharmaceutical formulations and serum samples.

3.3. Optimal experimental conditions

To improve analytical capability of the POB-fluorescence sensor for detecting TC, the impact of solvent, POB concentration, and incubation duration were examined. In terms of the poor solubility of POB in water, various organic solvents were tested to have comprehensive insight into their influence on its fluorescence properties. As exhibited in Fig. 3a, both protic and aprotic solvents experience distinct impact on the fluorescence intensity of the sensor. For example, ethanol gives the highest fluorescence quenching ratio (F_0/F) among the solvents under study. This can be interpreted based on the moderate polarity and dielectric constant of ethanol, which provide suitable environment for POB solvation. It is also among the most

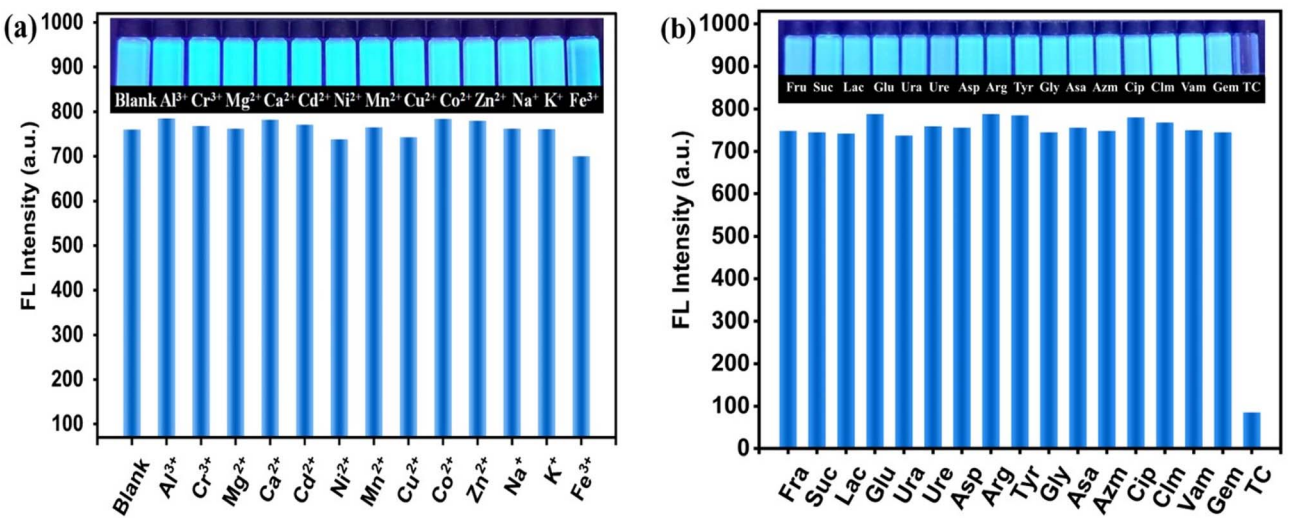

Fig. 2 Fluorescence intensity of 0.16 μM of POB at $\lambda_{ex} = 355$ nm and $\lambda_{em} = 418$ nm in the presence of 0.01 M of common interfering species: (a) metal ions and (b) biomolecules and antibiotics.

Open Access Article. Published on 09 March 2026. Downloaded on 4/15/2026 7:33:55 PM.
This article is licensed under a Creative Commons Attribution-NonCommercial 3.0 Unported Licence.

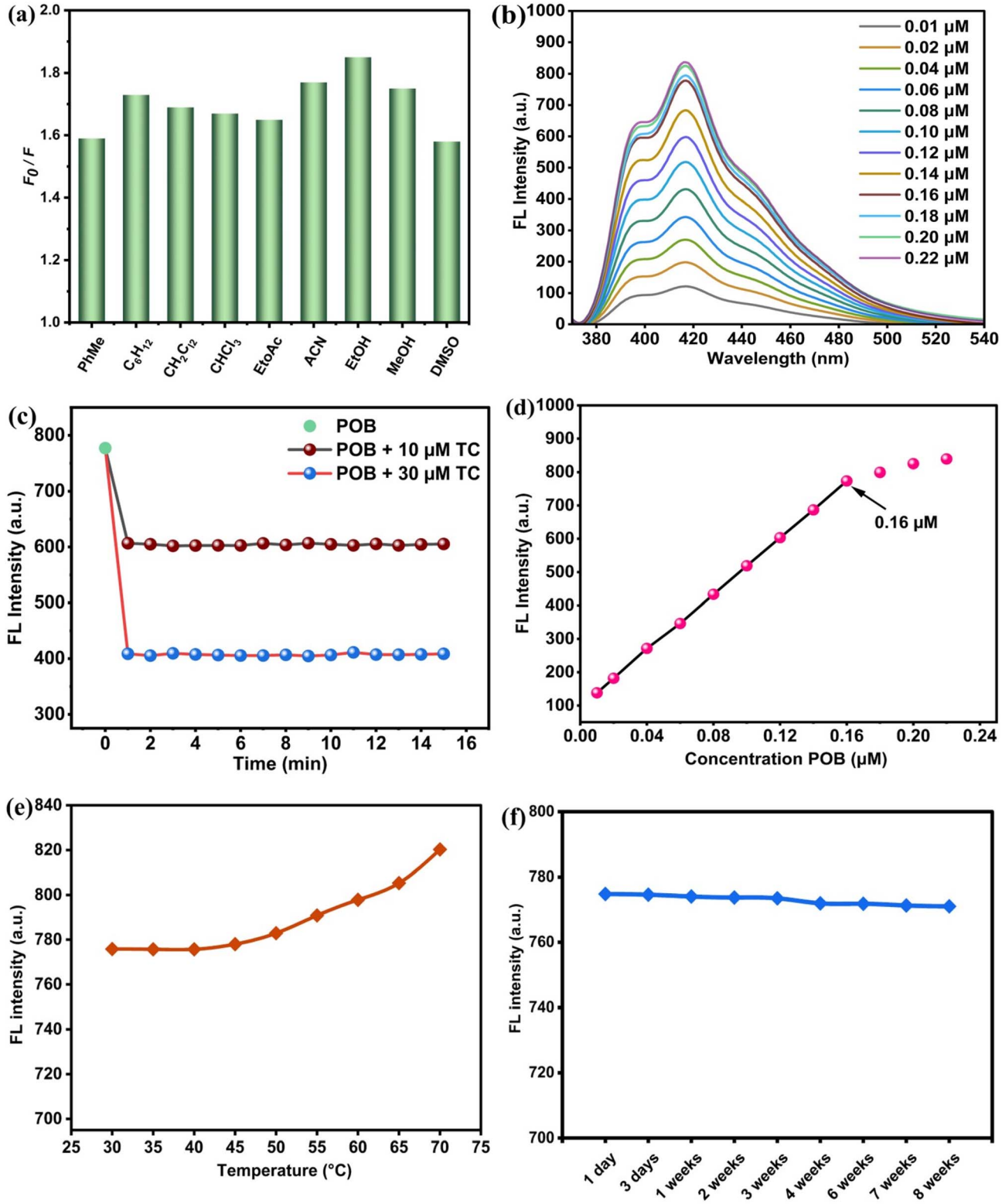

Fig. 3 (a) Effects of solvents on the fluorescence quenching ratio of 0.16 μM POB at $\lambda_{ex} = 355$ nm after addition of 30 μM of TC; (b) fluorescence spectra of different concentrations of POB; (c) fluorescence intensity of POB *versus* concentration; (d) impact of incubation time on the quenching fluorescence of 0.16 μM POB after addition of 10 and 30 μM of TC; (e and f) influence of temperature and storage time, respectively, on the fluorescence intensity of 0.16 μM of POB at $\lambda_{ex} = 355$ nm and $\lambda_{em} = 418$ nm.

© 2026 The Author(s). Published by the Royal Society of Chemistry

Open Access Article. Published on 09 March 2026. Downloaded on 4/15/2026 7:33:55 PM.
This article is licensed under a Creative Commons Attribution-NonCommercial 3.0 Unported Licence.

environmentally friendly options. It is concluded that ethanol can be chosen as the appropriate solvent for current analysis.

The concentration of the POB sensor is another effective factor that plays important role in fluorescence intensity and signal stability. As self-evidence, the high POB concentration leads to self-quenching and signal distortion. Contrarily, extremely low concentration results in poor detection. As a result, an appropriate concentration is essential and needs adjusting for providing accurate and precise fluorescence measurements. In Fig. 3b and c, fluorescence intensity increases linearly corresponding to its concentration up to 0.16 μM. The reduction of the intensity of fluorescence is noticeable at concentrations above 0.16 μM, which implies that this is the most appropriate sensor concentration that can be used to sustain a linear fluorescence signal. As a result, the fluorescence response of the sensor quenched by TC remains in the linear dynamic range that allows it to be quantified with high accuracy and reliability.

The incubation time is the prerequisite parameter for controlling the fluorescence intensity of the sensing system. The optimized incubation period is a vital parameter for providing a reproducible fluorescence signal and consistency within the experimental results. Moreover, this factor enables significant information about the concerning aggregation nature of the sensor, which directly impacts performance and analytical accuracy. In accordance with this, the responses received within a range of incubation durations were investigated. As shown in Fig. 3d, the quenching in fluorescence response was recorded at different incubation times before and after the addition of 10 and 30 μM of TC separately into the sensor solution. Noticeably, a rapid decline of the fluorescence intensity within 0–1 minute appears; afterwards, it becomes constant over time. The results indicated that the POB sensor has a high sensitivity and rapid response to TC and high stability for TC detection to ensure the accuracy of the results. Based on that, the choice of 1 minute was optimal as an incubation time.

The robustness and ruggedness of the POB sensor based on photoluminescence were further evaluated after studying the effectiveness of the key parameters, for instance, temperature and storage stability. Fig. 3e, demonstrates the impact of different temperatures that lie between 30 and 70 °C. It is also noticeable that the fluorescence intensity remains almost constant below 45 °C, suggesting a negligible influence of temperature variation on the POB performance. However, once the heating exceeded 45 °C, a noticeable increase in fluorescence intensity was obviously noted. This is because of the partial evaporation of ethanol in the medium. In the present work, to deal with the accuracy of detection and reproducibility of the experimental data points, all subsequent experiments were conducted at room temperature. The interesting notice is the storage stability time of POB that was assessed by collecting its fluorescence intensity records over different time intervals. Interestingly, to make the prepared working solution of POB stable for more than two months, the solution was kept in a refrigerator at 4 °C. As shown in Fig. 3f, the fluorescence intensity exhibited no notable variation, demonstrating excellent stability with only slight fluctuations over time. The results confirm that POB maintains its photoluminescent characteristics even after extended storage.

3.4. Quantitative analysis of TC

Under the established optimal conditions, the analytical feasibility of the proposed POB-based sensor for TC detection was evaluated. For this purpose, the fluorescence response of POB toward TC was investigated by measuring the emission intensity at various TC concentrations over the range 0–120 μM, as shown in Fig. 4a. A gradual decrease in fluorescence intensity was observed with increasing TC concentration, indicating the effective quenching of POB fluorescence upon interaction with

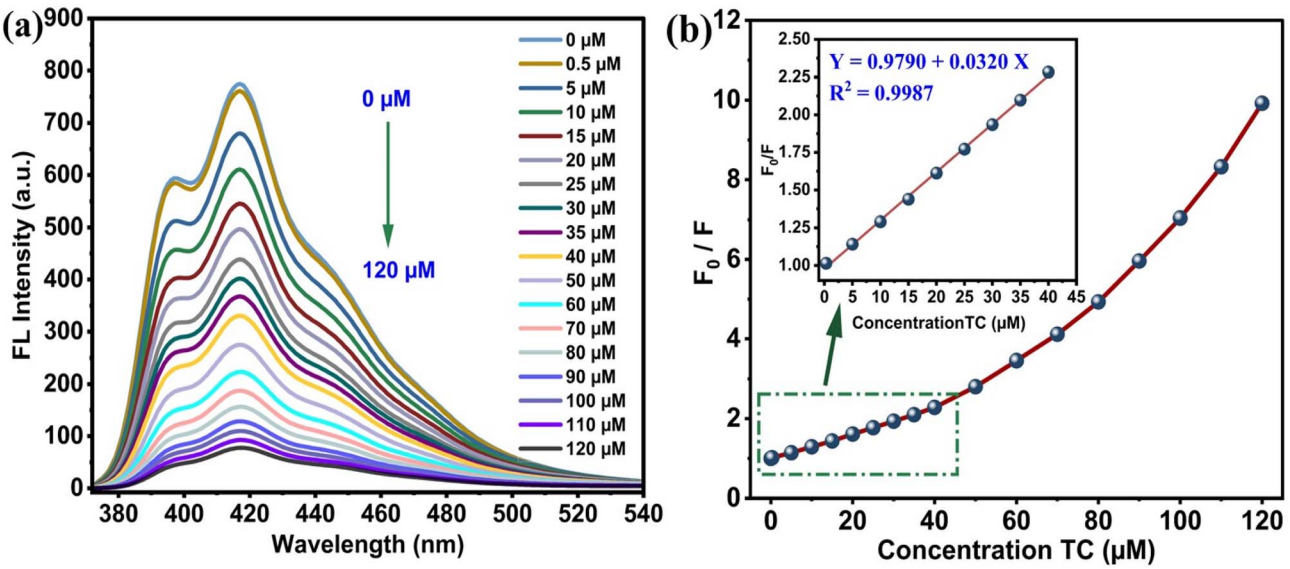

Fig. 4 (a) Spectra of fluorescence emission of 0.16 μM POB at different concentrations of TC (0–120 μM); (b) the relationship between F_0/F and TC concentrations (inset: shows the linear calibration curve between F_0/F and the concentration of TC in the range of 0.5–40 μM).

Open Access Article. Published on 09 March 2026. Downloaded on 4/15/2026 7:33:55 PM. This article is licensed under a Creative Commons Attribution-NonCommercial 3.0 Unported Licence.

TC. The correlation between the fluorescence intensity and the concentration of quencher can be best described by the Stern–Volmer equation.[52]

$$\frac{F_0}{F} = 1 + K_{sv}[TC] = 1 + K_q\tau_0[TC]$$

where F_0 and F represent the fluorescence intensities of POB in the absence and presence of TC, respectively; K_{sv} is the Stern–Volmer constant; K_q is the quenching rate; τ_0 denotes the fluorescence lifetime of the POB; and [TC] is the TC concentration. Fig. 4b shows a strong linear relationship between the FL quenching ratio (F_0/F) and TC concentration within the range of 0.5–40 μM. The calibration curve is described by the following linear regression equation:

$$\frac{F_0}{F} = 0.9790 + 0.0320[TC]$$

The correlation coefficient obtained from plot $R^2 = 0.9987$ indicates good correlation of the experimental data. The limit of detection (LOD) and limit of quantification (LOQ) were calculated using the following formula:[53,54]

$$LOD = 3.3\sigma/K_{sv} \text{ and } LOQ = 10\sigma/K_{sv}$$

hence, σ represents the standard deviation for ten repeated fluorescence measurements of blank solutions. The Stern–Volmer constant (K_{sv}) was determined from the linear calibration curve to be $3.2 \times 10^4\ M^{-1}$, and the LOD was calculated to be 0.143 μM, and the LOQ was computed to be 0.433 μM. The obtained results, especially the high K_{sv} value, demonstrate the excellent sensitivity and robustness of POB as a fluorescent sensor for the quantitative detection of TC.

Further study shows that reflection of the high sensitivity of POB based on a high K_{sv} value to low concentration of TC is impressive for practical implementation, especially in pharmaceutical and clinical analyses. This effective quenching outcome is in accordance with the observed linearity at relatively low concentrations.

3.5. Detection mechanism for TC by POB

The fluorescence of the POB was selectively quenched by TC, confirming its suitability as an efficient fluorescent sensor for TC detection. To investigate the possible quenching mechanism, a series of complementary experiments were used. The fluorescence response of the POB toward TC expressed by the correlation between F_0/F and TC concentrations (Fig. 4b) indicates that there are two distinct parts: a linear relationship at low concentration from 0.5 to 40 μM and a nonlinear curved behavior at high concentration in the range of more than 40 to 120 μM. This indicates that dynamic quenching is predominant at low concentrations, with a static quenching mechanism at higher concentrations.[5]

The study of optical characteristics of the sensor and quenching agent provides a deeper understanding about the sensing mechanism. A comparative inspection was carried out between the UV-vis absorption spectrum of TC and the fluorescence excitation spectrum of POB, as displayed in Fig. 5a. As can be seen, TC has a wide absorption spectrum over the range of 200–430 nm and was found to coincide with the fluorescence excitation spectrum of POB in the entire region of 200–400 nm. A significant spectral overlap is likely responsible for the reduction in fluorescence emission intensity of the POB, suggesting that the quenching mechanism is governed by the inner filter effect (IFE) and/or fluorescence resonance energy transfer (FRET). IFE is a purely optical phenomenon that occurs between the quencher and the fluorophore due to the quencher absorbing parts of the excitation or emission light of the fluorophore in the detection system. FRET involves

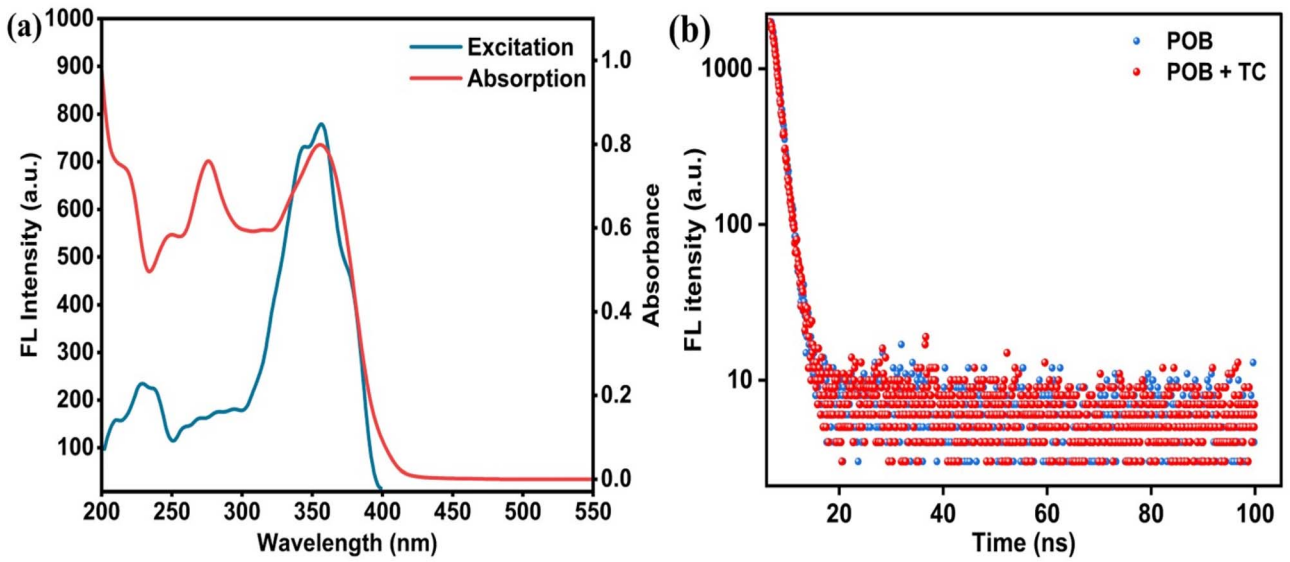

Fig. 5 (a) UV-Vis absorption spectrum of TC and fluorescence excitation spectrum of POB; (b) decay curves of POB in the absence and presence of TC.

© 2026 The Author(s). Published by the Royal Society of Chemistry

Open Access Article. Published on 09 March 2026. Downloaded on 4/15/2026 7:33:55 PM. This article is licensed under a Creative Commons Attribution-NonCommercial 3.0 Unported Licence.

Table 1 Results for the determination of TC in pharmaceutical products and human serum samples

Samples	Added (μM)	Found (μM)	Recovery[a] (%)	RSD (%)
Pharmaceutical formulation	4.0	3.91	97.75	1.23
	8.0	7.95	99.37	1.07
	16.0	16.35	102.18	1.43
Human serum	4.0	3.78	94.50	1.75
	8.0	7.81	97.62	2.31
	16.0	16.67	104.18	2.37

[a] Average of five determinations ($n = 5$).

nonradiative energy transfer from an excited fluorophore to quencher molecule and requires spectral overlap as well as close proximity, typically within a few nanometres. In contrast to IFE, FRET is based on the molecular level interactions between fluorophore and quencher.[38,55] The fluorescence quenching mechanism of POB upon interaction with TC is typically associated with combination factors, such as IFE, FRET, dynamic and static mechanisms. It has been known that IFE is capable of shortening the fluorescence of the sensor lifetime, but FRET cannot. To distinguish the type of quenching mechanism, the lifetimes of the fluorescence sensor were measured as illustrated in Fig. 5b. The average fluorescence lifetimes of POB were computed and are 2.26 ns and 1.58 ns, sequentially, in the absence and presence of TC. The remarkable decrease in the lifetime of the fluorophore sensor (POB) after the addition of TC shows the occurrence of dynamic quenching since the excited fluorophore collides with the quencher. In contrast, static quenching does not affect the lifetime, since it involves formation of a non-fluorescent ground-state complex.[56]

The Stern–Volmer equation is a popular quenching model applied for investigation efficiency and mechanism of the quenching process.[57] The high value of quenching constant ($K_{sv} = 3.2 \times 10^4\ M^{-1}$) reveals POB's fluorescence quenching efficiency toward TC. Beyond this, it suggests the substantial interaction between TC and POB, likely driven by effective energy transfer mechanisms. The computed quenching rate ($K_{eq} = 1.02 \times 10^{13}\ M^{-1}\ s^{-1}$) is much greater than the value of a diffusion-controlled (dynamic) quenching process ($1.0 \times 10^{12}\ M^{-1}\ s^{-1}$). Ultimately, this confirmation reveals the quenching mechanism, which is predominantly static.

3.6. Analysis of TC in real samples

The analytical applicability of the POB-fluorescence sensor was studied for detecting TC in different sample matrices, including pharmaceutical formulations and serum samples. A range of TC concentrations within the established calibration curve was explored. The determination of TC concentration in capsule samples was quantified using a direct measurement approach, while in serum samples, concentration was assessed by using a spiking human serum. The data points presented in Table 1 interpret the recovery rates ranging from 97.75% to 102.18% for pharmaceutical product samples and 94.50% to 104.18% for serum samples. Additionally, the method reveals POB-fluorescence has good reproducibility, with relative standard deviation (RSD) smaller than 3% in both cases. The statistical analysis outcomes confirm the application of the POB-fluorescence platform for the detection of TC in pharmaceutical formulations and human serum samples.

3.7. Evaluation of environmental impact

The implementation of green chemistry guidelines is essential in the context of reducing the adverse effects of dangerous chemicals on the environment and helps develop environmentally analytical strategies. These standards encourage the use of solvents and reagents that are safer and reduce the generation of waste that is dangerous and promote the use of renewable materials along with improved laboratory safety procedures.[58] The eco-friendliness profile of the fluorometric method was estimated through using two metric tools, namely, the Analytical Greenness Metrics for Sample Preparation (AGREEprep) and the Blue Applicability Grade Index (BAGI). Both tools assess sample preparation steps and overall procedures to determine how well they align with green chemistry standards.

AGREEprep software is a breakthrough tool developed by Pena-Pereira *et al.* in 2022 for investigating the environmental impact of sample preparation procedures through using ten factors. The key factors include, solvent, material, and reagent selection, as well as waste, energy, sample size, and throughput, quantifying each on a standardized 0–1 scale. The overall evaluation scores indicate the greenness rating that can be portrayed by color-codes or numerically. This shape of illustration facilitates successful comparison of sample preparation techniques from an environmental perspective.[59–62]

In 2023, BAGI was introduced as a new software tool for evaluating the practicality and applicability of analytical methods according to the principles of White Analytical Chemistry proposed by Nowak *et al.* The software relies on ten defined criteria to produce a pictogram and a numerical score reflecting the functional quality of a given method. A sequential blue color scale, from dark to light, indicates the level of compliance with these criteria. Methods with a total score above 60 are regarded as practical and suitable for routine use.[63,64]

As depicted in Fig. 6a and b, AGREEprep was employed to estimate the environmental impact of different sample preparation procedures for determining TC in pharmaceutical formulations and serum samples. The figures reveal that the procedures were conducted in a laboratory setting, requiring

Open Access Article. Published on 09 March 2026. Downloaded on 4/15/2026 7:33:55 PM.
This article is licensed under a Creative Commons Attribution-NonCommercial 3.0 Unported Licence.

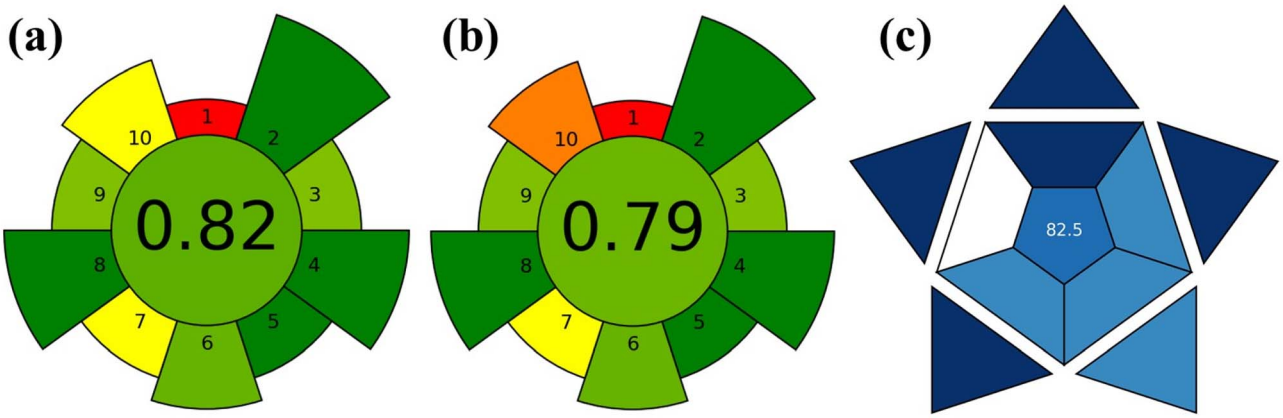

Fig. 6 Presents the greenness evaluation of the proposed method. (a and b) Illustrate the AGREEprep results for the sample preparation methodology applied to pharmaceutical products and serum samples. (c) Displays the BAGI assessment used to examine environmental impact of the fluorometric method.

the collection and transportation of samples (*ex situ*) and semi-automated systems for sample preparation. The primary difference between the two sample preparation procedures lies in the type and quantity of solvents used. Environmentally, ethanol is considered a recommended solvent owing to its less harmful, biodegradable nature and availability from renewable feedstocks.[65] Therefore, ethanol was employed in the sample handling of pharmaceutical specimens, thus lowering environmental impact and promoting labour safety. Acetonitrile was applied for precipitation of proteins from human serum and is categorized as a problematic solvent due to its primarily comes from petroleum-based resources, which decreases the score of greenness. However, the use of fluorescence instrumentation, which consumes low electrical energy and small quantities of reagents per analysis, helps to reduce the generation of chemical wastes, improving the eco-friendly nature of such analysis protocols. The result of the AGREEprep assessment shown in Fig. 6a for pharmaceutical formulations, with a score of 0.82, and in Fig. 6b for serum samples, with a score of 0.79, highlights the green nature of the sample preparation methodology.

The practicability and applicability of the proposed fluorometric method were examined using the BAGI software. The method targets a single analyte and relies on readily available reagents and simple laboratory equipment. It processes more than ten samples per hour and allows preparation of about thirty samples at the same time. Moreover, the procedure does not require any preconcentration steps, and the fluorescence sensing procedure presented in this work using a commercially available fluorophore does not require any synthesis steps. The analysis used only 50 μL of serum or less than 0.1 g of TC capsule material, and all steps were performed semi-automatically. As shown in Fig. 6c, the method received a BAGI score of 82.5, indicating environmental practicability and applicability for routine analysis.

Table 2 Comparison of characteristics of different analytical methods for TC detection

Main precursor	Sensor type	Synthetic method	Time and temperature	Linear range (μM)	LOD (μM)	QY%	Ref.
$Ca(NO_3)_2$, L-cysteine	CdSQDs	Chemical precipitation	4 h at 50 °C	15–600	7.78	69	66
Milk	N-doped CDs	Hydrothermal	4 h at 180 °C	2–200	0.6	10	67
O-phenylene diamine, glyoxal	Carbon dots (CDs)	Amine–aldehyde condensation	3 h at 25 °C	10–400	6	—	68
Sodium tungstate, cysteine	WS_2QDs	Hydrothermal	10 h at 200 °C	0.1–10	0.039	9.6	55
$Eu(NO_3)_3 \cdot 6H_2O$ citric acid melamine, formaldehyde	Eu-CDs	Hydrothermal	10 h at 220 °C	0–100	6.9	10.81	69
Waste tea, HNO_3, Na_2CO_3	CDs	Chemical oxidation	6 h at ∼100 °C	0–7.2	0.09	2.47	70
Citric acid, TEOS[a], APTES[b]	GQDs-SMIPs[c]	Sol–gel polymerization	0.5 h at 200 °C	15–120	3.55	_	71
$AgNO_3$, ammonia, glucose, β-cyclodextrin	AgNPs	Chemical reduction	0.5 h, ∼100 °C	0.12–12.47	1.31	_	72
$Zn(CH_3COO)_2 \cdot 2H_2O$, BTC[d]	Zn-MOF	Solvothermal	16 h at 180 °C	0–17	0.014	_	73
1,4-Di-2-(5-phenyloxazolyl)-benzene (POB)	POB Commercial dye	No synthesis	≤10 min at 25 °C	0.5–40	0.143	84	This work

[a] Tetraethoxysilane. [b] 3-Aminopropyltriethoxysilane. [c] Graphene quantum dots coated with silica molecularly imprinted polymers. [d] 1,3,5-Benzenetricarboxylic acid.

© 2026 The Author(s). Published by the Royal Society of Chemistry

Open Access Article. Published on 09 March 2026. Downloaded on 4/15/2026 7:33:55 PM. This article is licensed under a Creative Commons Attribution-NonCommercial 3.0 Unported Licence.

The AGREEprep and BAGI assessments demonstrate strong environmental performance of the established method regarding the use of solvent, sample preparation steps, and the overall analytical procedure. Moreover, the validity and environmental compatibility of the method, compared with the extensive reported methods for TC analysis, are illustrated in Table 2. As shown in the table, most of the previously documented sensors, including CDs, MOFs, and MIP-based systems, rely on intensive synthesis procedures that require long reaction times, high temperatures, considerable energy usage, low quantum yields, and sometimes the use of multiple organic precursors or solvents. These factors significantly reduce their environmental friendliness when compared with the POB fluorescent probe. In contrast, the fluorescence sensing strategy developed in this work uses a commercially available fluorophore, operates at room temperature with minimal energy input, and offers a simple and time-efficient approach. Moreover, it provides a broad linear range, an acceptable detection limit, and reliable performance in serum and pharmaceutical samples, making it well suited for routine analysis and green analytical applications.

4. Conclusions

In summary, the fluorescence detection platform based on strong fluorescent 1,4-di-2-(5-phenyloxazolyl)-benzene (POB) was established, characterized by its simplicity, cost-effectiveness, and eco-friendliness for the detection of TC in pharmaceutical formulation and human serum. The sensor demonstrated high selectivity and sensitivity for quantification of TC and minimal response for common interferences such as metal ions, biomolecules, and other antibacterial compounds. The introduction of TC efficiently quenches the POB's fluorescence mainly through the inner filter effect mechanism. The proposed fluorometric platform displayed a satisfactory recovery rate and relative standard deviation for the detection of TC in different matrices. The environmental suitability of the method was confirmed *via* the green assessment tools such as AGREEprep and BAGI, which support its sustainable nature. Overall, the POB fluorescence sensor shows high quantum yield, good resistance to photobleaching, and offers a fast, accurate, and environmentally friendly method for routine TC determination in pharmaceutical analysis and clinical applications.

Author contributions

Muhammad S. Mustafa: conceptualization, methodology, investigation, validation, data curation, formal analysis, software, visualization, writing – original draft; Wrya O. Karim: supervision, resources, project administration, writing – review & editing.

Conflicts of interest

The authors declare no competing interests.

Data availability

Data will be available upon request.

Acknowledgements

The authors gratefully acknowledge the University of Sulaimani for supporting this research.

References

1 T. Gil-Gil and B. A. Berryhill, *Antimicrob. Agents Chemother.*, 2025, **69**, 1–9.
2 A. Ishak, N. Mazonakis, N. Spernovasilis, K. Akinosoglou and C. Tsioutis, *J. Antimicrob. Chemother.*, 2025, **80**, 1–17.
3 X. Dou, Q. Wu, S. Luo, J. Yang, B. Dong, L. Wang, H. Qu and L. Zheng, *Talanta*, 2024, **271**, 125702–125709.
4 K. Phomai, S. ang Supharoek, J. Vichapong, K. Grudpan and K. Ponhong, *Talanta*, 2023, **252**, 123852–123862.
5 K. Mili, Z. Hsine, Y. Chevalier, G. Ledoux and R. Mlika, *Solid State Commun.*, 2023, **360**, 115040–115051.
6 O. B. A. Shatery, K. F. Kayani, M. S. Mustafa and S. J. Mohammed, *Res. Chem. Intermed.*, 2024, **50**, 2291–2306.
7 M. Khawla, H. Zouhour, C. Yves, H. Souhaira and M. Rym, *Opt. Mater.*, 2022, **125**, 112103–112112.
8 H. Wu, Y. Chen, M. Xu, Y. Ling, S. Ju, Y. Tang and C. Tong, *Sci. Total Environ.*, 2023, **860**, 160533–160544.
9 A. N. Berlina, A. V. Bartosh, A. V. Zherdev, C. Xu and B. B. Dzantiev, *Antibiotics*, 2018, **7**, 1–11.
10 S. Liu, G. Zhao, H. Zhao, G. Zhai, J. Chen and H. Zhao, *Sci. Total Environ.*, 2017, **599–600**, 298–304.
11 C. Saenjum, N. Pattapong, T. Aunsakol, T. Pattananandecha, S. Apichai, H. Murakami, K. Grudpan and N. Teshima, *J. Food Compos. Anal.*, 2022, **105**, 104215–104221.
12 S. ang Supharoek, K. Ponhong, B. Weerasuk, W. Siriangkhawut and K. Grudpan, *J. Iran. Chem. Soc.*, 2020, **17**, 2385–2395.
13 R. M. Khaleel and D. H. Mohammed, *J. Phys.: Conf. Ser.*, 2020, **1664**, 12084–12097.
14 R. Widiastuti and Y. Anastasia, *IOP Conf. Ser.: Earth Environ. Sci.*, 2022, **1001**, 1–5.
15 M. N. Alnassrallah, N. Z. Alzoman and A. Almomen, *Sci. Rep.*, 2022, **12**, 1–14.
16 E. Butovskaya, A. M. Carrillo Heredero, G. Segato, E. Faggionato, M. Borgia, D. Marchis, S. Menotta and S. Bertini, *Food Addit. Contam.,:Part A*, 2024, **41**, 601–609.
17 M. Rahimi Moghadam, B. Zargar and S. Rastegarzadeh, *J. AOAC Int.*, 2021, **104**, 999–1004.
18 H. Saleh, M. Elhenawee, E. M. Hussien, N. Ahmed and A. E. Ibrahim, *Food Anal. Methods*, 2021, **14**, 36–43.
19 H. zhi Tang, Y. hui Wang, S. Li, J. Wu, Z. xian Gao and H. ying Zhou, *J. Food Sci. Technol.*, 2020, **57**, 2884–2893.
20 S. Zergiebel, N. Ueberschaar and A. Seeling, *Food Chem.*, 2023, **402**, 134270–134280.
21 J. Pang, H. Chen, H. Guo, K. Lin, S. Huang, B. Lin and Y. Zhang, *J. Hazard. Mater.*, 2024, **469**, 133768–133781.

© 2026 The Author(s). Published by the Royal Society of Chemistry

Open Access Article. Published on 09 March 2026. Downloaded on 4/15/2026 7:33:55 PM. This article is licensed under a Creative Commons Attribution-NonCommercial 3.0 Unported Licence.

22 Á. Grande-Martínez, D. Moreno-González, F. J. Arrebola-Liébanas, A. Garrido-Frenich and A. M. García-Campaña, *J. Pharm. Biomed. Anal.*, 2018, **155**, 27–32.
23 R. E. Gavilán, C. Nebot, M. Veiga-Gómez, P. Roca-Saavedra, B. Vazquez Belda, C. M. Franco and A. Cepeda, *J. Anal. Methods Chem.*, 2016, **2016**, 1–8.
24 Y. Feng, W. J. Zhang, Y. W. Liu, J. M. Xue, S. Q. Zhang and Z. J. Li, *Molecules*, 2018, **23**, 1953–1966.
25 L. Devkota, L. T. Nguyen, T. T. Vu and B. Piro, *Electrochim. Acta*, 2018, **270**, 535–542.
26 C. E. C. Lopes, L. V. de Faria, D. A. G. Araújo, E. M. Richter, T. R. L. C. Paixão, L. M. F. Dantas, R. A. A. Muñoz and I. S. da Silva, *Talanta*, 2023, **259**, 124536–124544.
27 L. Zhang, M. Yin, X. Wei, Y. Sun, Y. Luo, H. Lin, R. Shu and D. Xu, *Bioelectrochemistry*, 2024, **157**, 108668–108675.
28 D. Moreno-González, I. Lupión-Enríquez and A. M. García-Campaña, *Electrophoresis*, 2016, **37**, 1212–1219.
29 G. Islas, J. A. Rodriguez, I. Perez-Silva, J. M. Miranda and I. S. Ibarra, *J. Anal. Methods Chem.*, 2018, **2018**, 1–7.
30 Y. J. Peng, M. H. Liu, J. H. Zhao, H. C. Yuan, Y. Li, J. J. Tao and H. Q. Guo, *Guangpuxue Yu Guangpu Fenxi*, 2017, **37**, 3736–3742.
31 A. Desmarchelier, S. Anizan, M. Minh Tien, M. C. Savoy and C. Bion, *Food Addit. Contam.,:Part A*, 2018, **35**, 686–694.
32 R. Batool, N. Riaz, M. T. Waseem, S. Nawazish, U. Farooq, C. Yu and S. A. Shahzad, *ACS Omega*, 2022, **7**, 1057–1070.
33 J. Khan, *J. Fluoresc.*, 2024, **34**, 2485–2494.
34 J. Hu, S. Liao, Y. Bai and S. Wu, *J. Environ. Chem. Eng.*, 2024, **12**, 112595–112602.
35 Z. Li, Y. Wang, J. Chen, L. Zhang, Y. Hua, D. Huang, H. Guo and X. Qiu, *Opt. Mater.*, 2024, **150**, 115227–115235.
36 W. Hou, C. Liang, Y. Li, C. Shao, Y. Zheng, Z. Li, S. Pu and C. Fan, *J. Photochem. Photobiol., A*, 2025, **466**, 116411–11621.
37 N. Zhao, Y. Wang, S. Hou and L. Zhao, *Microchim. Acta*, 2020, **187**, 351–361.
38 F. Yan, Z. Sun, J. Pang, Y. Jiang and W. Zheng, *Dyes Pigm.*, 2020, **183**, 108673–110879.
39 Q. Chen, H. Zhang, H. Sun, Y. Yang, D. Zhang, X. Li, L. Han, G. Wang and Y. Zhang, *Food Chem.*, 2024, **442**, 138383–138394.
40 Z. Gan, X. Hu, X. Xu, W. Zhang, X. Zou, J. Shi, K. Zheng and M. Arslan, *Food Chem.*, 2021, **354**, 129501–129509.
41 L. Liu, Q. Chen, J. Lv, Y. Li, K. Wang and J. R. Li, *Inorg. Chem.*, 2022, **61**, 8015–8021.
42 V. Mishra, A. Patil, S. Thakur and P. Kesharwani, *Drug Discovery Today*, 2018, **23**, 1219–1232.
43 N. Zhao, Y. Wang, S. Hou and L. Zhao, *Microchim. Acta*, 2020, **187**, 1–10.
44 H. Hu, Y. Wu and X. Gong, *Small*, 2024, **20**, 1–31.
45 L. E. Kreno, K. Leong, O. K. Farha, M. Allendorf, R. P. Van Duyne and J. T. Hupp, *Chem. Rev.*, 2012, **112**, 110–1125.
46 K. F. Kayani, S. J. Mohammed, N. N. Mohammad, G. H. Abdullah, D. A. Kader and N. S. Hamad, *Food Control*, 2024, **164**, 110611–110623.
47 S. T. Alsharif, S. l. Alaqel, A. H. Almalki, M. A. Algarni, R. M. Alnemari, M. H. Abduljabbar and A. H. Abdelazim, *Spectrochim. Acta, Part A*, 2024, **309**, 1–5.
48 J. Raúl, M. Sandoval, M. Enrique, M. Rosas, E. M. Sandoval, M. Enrique, M. Rosas, M. Moisés and M. Velasco, *IntechOpen*, 2023, **1**, 61–78.
49 S. O. Fakayode, C. Lisse, W. Medawala, P. N. Brady, D. K. Bwambok, D. Anum, T. Alonge, M. E. Taylor, G. A. Baker, T. F. Mehari, J. D. Rodriguez, B. Elzey, N. Siraj, S. Macchi, T. Le, M. Forson, M. Bashiru, V. E. Fernand Narcisse and C. Grant, *Appl. Spectrosc. Rev.*, 2024, **59**, 1–89.
50 J. Khan, *J. Fluoresc.*, 2023, **1**, 1573–4994.
51 A. M. Brouwer, *Pure Appl. Chem.*, 2011, **83**, 2213–2228.
52 F. Hu, Q. Fu, Y. Li, C. Yan, D. Xiao, P. Ju, Z. Hu, H. Li and S. Ai, *Food Chem.*, 2024, **431**, 137097–137105.
53 Y. N. Wang, S. D. Wang, L. L. Yang, Y. F. Zhao and Q. F. Yang, *J. Solid State Chem.*, 2020, **289**, 121519.
54 S. B. Suryawanshi, P. G. Mahajan, A. J. Bodake, G. B. Kolekar and S. R. Patil, *Spectrochim. Acta, Part A*, 2017, **183**, 232–238.
55 J. Ge, D. Ma, G. Duan, Z. Yan, L. Yang, D. Yang and R. Cai, *Anal. Chim. Acta*, 2022, **1221**, 1–7.
56 S. R. Lodha, J. G. Merchant, A. J. Pillai, A. H. Gore, P. O. Patil, S. N. Nangare, G. G. Kalyankar, S. A. Shah, D. R. Shah and S. P. Patole, *Heliyon*, 2024, **10**, e41020.
57 Y. Fan, W. Qiao, W. Long, H. Chen, H. Fu, C. Zhou and Y. She, *Spectrochim. Acta, Part A*, 2022, **274**, 121033–121041.
58 M. Sajid and P. Justyna, *Talanta*, 2022, **238**, 123046–123056.
59 K. F. Kayani, O. B. A. Shatery, M. S. Mustafa, A. H. Alshatteri, S. J. M. De and S. B. Aziz, *RSC Adv.*, 2024, **14**, 5012–5021.
60 M. S. Mustafa, N. N. Mohammad, F. H. Radha, K. F. Kayani, O. Ghareeb and S. J. Mohammed, *RSC Adv.*, 2024, **14**, 16045–16055.
61 W. Wojnowski, M. Tobiszewski, F. Pena-Pereira and E. Psillakis, *TrAC, Trends Anal. Chem.*, 2022, **149**, 116553–116562.
62 F. Pena-pereira, M. Tobiszewski, W. Wojnowski and E. Psillakis, *Adv. Sample Prep.*, 2022, **3**, 100025–100032.
63 N. Manousi, W. Wojnowski, J. Płotka-Wasylka and V. Samanidou, *Green Chem.*, 2023, **25**, 7598–7604.
64 K. F. Kayani and A. M. Abdullah, *J. Food Compos. Anal.*, 2024, **135**, 106577–106588.
65 D. Prat, A. Wells, J. Hayler, H. Sneddon, C. R. Mcelroy, S. Abou-shehada and P. J. Dunn, *Green Chem.*, 2016, **18**, 288–296.
66 S. K. Anand, U. Sivasankaran, A. R. Jose and K. G. Kumar, *Spectrochim. Acta, Part A*, 2019, **213**, 410–415.
67 B. Al-hashimi, K. M. Omer and H. S. Rahman, *Arabian J. Chem.*, 2020, **13**, 5151–5159.
68 Y. Yan, J. Hui, R. Sheng, Y. Fang and C. Zhi, *Anal. Chim. Acta*, 2019, **1063**, 144–151.
69 Y. Sang, K. Wang, X. Kong, F. Cheng, C. Zhou and W. Li, *Sens. Actuators, B*, 2022, **362**, 131780.
70 D. B. Gunjal, Y. M. Gurav, A. H. Gore, V. M. Naik, R. D. Waghmare, C. S. Patil, D. Sohn, P. V Anbhule, R. V Shejwal and G. B. Kolekar, *Opt. Mater.*, 2019, **98**, 109484.
71 K. M. Kelani, M. A. Hegazy, A. M. Hassan and A. H. Nadim, *Sci. Rep.*, 2025, **15**, 1–12.
72 P. Wang, T. Wu and Y. Zhang, *Talanta*, 2016, **146**, 175–180.

© 2026 The Author(s). Published by the Royal Society of Chemistry

73 S. Sh, M. Ameen, F. O. Qasim, H. S. Alhasan, K. H. H. Aziz and K. M. Omer, *Appl. Mater. Interfaces*, 2023, **15**, 46098–46107.

Open Access Article. Published on 09 March 2026. Downloaded on 4/15/2026 7:33:55 PM.
This article is licensed under a Creative Commons Attribution-NonCommercial 3.0 Unported Licence.